Application of high specific surface area Ag/AgCl/TiO_2 coupled photocatalyst fabricated by fused filament fabrication

Zheng-Rong Yang
Tamkang University
Po-Ching Lee
Tamkang University
Chun-Yu Kuo
Tamkang University
Chung-Hao Shin
Tamkang University
Ching-Bin Lin (cblin@mail.tku.edu.tw)
Tamkang University

Research Article

Keywords: silver chloride, fused filament fabrication, methyl blue dye, Escherichia coli, reliability

Posted Date: January 24th, 2022

DOI: https://doi.org/10.21203/rs.3.rs-1264746/v1

Version of Record: A version of this preprint was published at The International Journal of Advanced Manufacturing Technology on March 17th, 2022. See the published version at https://doi.org/10.1007/s00170-022-09038-x.

Abstract

This study used a three-dimensional (3D) printing process to develop a Ag/AgCl/TiO_2 coupled photocatalyst with a large specific surface area. We examined the catalytic ability of this photocatalyst in methyl blue dye degradation and *Escherichia coli* sterilization as well as the reliability of its repeated use. A TiO_2 module was constructed of fuse filament [through fused filament fabrication (FFF)], and the adopted 3D printing filament was composed of anatase (TiO_2) nanoparticles, stearic acid, wax, and a plasticizer. The green compact of the TiO_2 module was subjected to solvent debinding, thermal debinding, and sintering to obtain a basic structure that was subsequently coupled with AgCl through a precipitation reaction. Ultraviolet radiation was used for the photoreduction of the coupled product to obtain a Ag/AgCl/TiO_2 photocatalyst coupling module. This photocatalyst can effectively degrade methylene blue (MB) dye and disinfect *E. coli*. The degradation of MB dye and sterilization of *E. coli* were conducted under visible and ultraviolet light. The degradation of MB dye by Ag/AgCl/TiO_2 was a first-order reaction. In addition, this catalyst could retain its MB dye degradation rate (95%) for five cycles. *E. coli* was sterilized using the prepared photocatalyst in a 120-min test, and this sterilization was a hyperbolic reaction. The photocatalytic module manufactured in this study through FFF can degrade pollutants in water has durability and retains reliability after repeated use.

1. Introduction

The textile dyeing and finishing industry discharges a large quantity of industrial waste that contains numerous chemically toxic pigments and dyes into bodies of water, which results in their pollution and causes serious harm to humans and the natural environment [1]. Traditional industrial wastewater treatment methods include coagulation and biological treatment; however, industrial wastewater treated using these methods does not meet discharge standards. Traditional drinking water disinfection usually involves chlorination procedures. Chlorination is the addition of chlorine or chlorine byproducts to drinking water for disinfection. Although this method has a strong disinfection effect, chlorinated drinking water frequently has a peculiar smell and may even contain some potentially toxic or mutagenic products, such as trihalomethane and chloroform, which are often carcinogenic. Photocatalysis technology enables the nontoxic, nonpolluting, and efficient treatment of dyes in industrial wastewater and the sterilization of drinking water [2]. For example, anatase (TiO_2) nanoparticles can generate electron–hole pairs after absorbing a certain wavelength of photon energy. Holes interact with water molecules to form ($OH^•$) free radicals with a strong oxidizing ability. Electrons and oxygen combine to produce ($O_2^{-•}$) free radicals. These free radicals can degrade dyes and disinfect bacteria. Anatase nanoparticles are widely used photocatalysts with high photocatalytic efficiency and photocatalytic activity [3]. However, because the energy gap of anatase is approximately 3.2 eV, this photocatalyst is only suitable for use with ultraviolet light with a wavelength of less than 380 nm and is rarely used with sunlight. The ultraviolet light absorption band covers only 5% of the solar spectrum; thus, the applicability of anatase nanoparticles as a catalyst is limited [4]. Consequently, some studies have developed new photocatalyst materials for utilization under sunlight. For example, the AgX (X = Cl, Br) photocatalyst

forms silver radicals after being irradiated. Because of the surface plasmon resonance effect of silver clusters, the AgX photocatalyst exhibits excellent photocatalytic activity under visible light [5]. According to Kakuta et al. [6], Ag (silver clusters)/AgCl, which can absorb visible light, has a stronger photocatalytic effect than does nitrogen-doped TiO_2. Ag/AgCl almost eliminates the proliferation ability of bacteria in a short time and causes cell death. In addition, to achieve effective photocatalysis under visible light, photocatalysts containing AgCl and metal or nonmetal oxides, such as Ag/AgCl/WO_3 [7], Ag/AgCl/MCM-41 [8], Ag/AgCl/TiO_2 [9], Ag/AgI/Al_2O_3 [10], Ag/AgCl/ZnO [11], and AgCl/rGO [12], Ag/AgCl/SiO_2/GO [13], Ag/AgCl-NC[14] and Ag/AgCl@MIL-88A(Fe)[15] have been developed. Some studies have indicated that the combination of TiO_2 with Ag/AgCl can strengthen the catalytic effect of visible light and increase the stability of degradation [16-20]. Yang et al. [9] synthesized the Ag/AgCl/TiO_2 coupled photocatalyst by using the sol–gel method and the hydrothermal method combined with the ion exchange method, and degraded Rose Bengal under xenon lamp irradiation. the Ag/AgCl/TiO_2 coupled photocatalyst is superior to TiO_2 and Ag/TiO_2 because it has a lower recombination rate of electrons and holes.

Zhang et al. [16] synthesized the Ag/AgCl/TiO_2 coupled photocatalyst by using a solvothermal method. Under visible light irradiation, this photocatalyst exhibits high photocatalytic activity and can quickly sterilize *Escherichia coli*. This phenomenon occurs because after Ag/AgCl is coupled with TiO_2, the recombination rate of electrons and holes decreases, and the minority carrier separation rate increases during the photocatalytic reaction, as indicated by steady-state and transient photoluminescence spectra. According to Shah et al. [18], when Ag/AgCl/TiO_2 is used for the photocatalytic degradation of methyl orange under visible light, CuO can be mixed into the methyl orange solution as an additional catalyst (catalysis occurs through electron absorption). According to Guo et al. [7], Ag/AgCl/TiO_2 coupled photocatalysts prepared through the deposition–precipitation method and photoreduction method have high photocatalytic activity and can effectively degrade 4-chlorophenol and hexavalent chromium ions under visible light irradiation. The high photocatalytic activity of these photocatalysts is attributed to the surface plasmon resonance effect of silver clusters. According to Guan et al. [21], when the Ag/AgCl/ZIF-8/TiO_2 photocatalyst coating cotton fabric is used, the photocatalytic degradation of methylene blue (MB) solution can reach 98.5% in 105 min under visible light irradiation. The kinetic constant of this first-order photocatalytic degradation is 0.0332 min^{-1}. In addition, this photocatalyst can maintain a degradation rate of approximately 85% after three degradation cycles. However, although a particle suspension of a Ag/AgX (X = Cl, Br)/TiO_2 coupled photocatalyst has high photocatalytic efficiency, it has several drawbacks. First, after the Ag/AgCl/TiO_2 catalyst is used to degrade dyes, it must be subjected to complicated filtration and centrifugal separation before being reused, which limits its practical applicability. Second, if Ag/AgCl/TiO_2 particles cannot be recycled effectively, they flow into water sources and land, thereby causing secondary pollution.

Some ceramic three-dimensional (3D) printing technologies, such as fused filament fabrication (FFF), ceramic extrusion deposition, binder jet deposition, powder sintering deposition, paste extrusion deposition, selective laser sintering, direct ceramic inkjet, and photopolymerization, have been developed

to manufacture 3D ceramic structures. FFF can be used to create ceramic structures with a large specific area. The manufacturing process of a ceramic fuse involves feeding a continuous filament into a heated nozzle and then melting, extruding, depositing, and printing this molten filament on the printing tablet. The continuous filament used in ceramic FFF is a thermoplastic material that contains ceramic particles; short fibers; or other ingredients, such as wax and stearic acid. After the 3D printing of a green embryo, the embryo is moved into solvent or heating degreasing equipment to remove the thermoplastic and organic components and then sintered to densify the printed workpiece to form a block structure. In the present study, fused filaments were used to manufacture a 3D-printed module of Ag/AgCl/TiO_2 with a large specific surface area. This module was used for the degradation of the azo dye Orange II and the sterilization of environmental *E. coli*. Moreover, the durability and reuse reliability of the Ag/AgCl/TiO_2 coupled photocatalyst module were tested.

2. Experimental

2.1 Feedstock material for 3D printing

In FFF, a continuous filament is used to print 3D objects, and a continuous filament printing line is manufactured using an extrusion molding machine. The filament fabricated in this study comprised anatase powder (50%) with 20-nm particles, high-density polyethylene (40%), wax (4.5%), stearic acid (1.5%), and a plasticizer (4%).

These materials were stirred in a Banbury mixer (Well Shyang Machinery Co., LTD., SBI-3L, R.O.C.) at 50 rpm and 175°C for 30 min to ensure that all the ingredients were completely melted and mixed evenly. The obtained mixture was then cut into pellets, fed into a single-screw extruder (Der-Hsin Plastic Machinery, R.O.C) with a screw speed of 30 rpm, melted, and extruded to form linear filaments. The exit temperature of the extrusion molding machine was 160°C, and the diameter of the exit of the extrusion die was 1.75 mm. The diameter of the filament after extrusion was 1.70-1.80 mm, and the ovality of the filament was 0.1 mm (an ovality of 0 represents a true circle).

2.2 Ceramic fused thread of 3D printing head, module design, and manufacturing

The fabricated Ag/AgCl/TiO_2 coupled photocatalyst module comprised a large specific surface area Ag/AgCl/TiO_2 coupled photocatalyst cylinder, a stirring shaft, and polylactic acid (PLA) upper and lower pressing plates. The central circular hole of the PLA pressing plate contained internal threads that could be connected to the external threads of the rotating shaft. The Ag/AgCl/TiO_2 coupled photocatalyst module is displayed in Fig. 1(a). The highly specific surface area Ag/AgCl/TiO_2-coupled photocatalytic cylinder was adapted for structural strength and flow-field design. The assembly process of the Ag/AgCl/TiO_2 coupled photocatalyst module is described in the following text. First, the stirring rotating shaft is passed through the highly specific surface area AgCl/TiO_2-coupled photocatalytic cylinder, the internal thread is screwed into the circular hole in the lower PLA plate, and then the upper PLA plate is

placed in the stirring shaft on the upper surface of the highly specific surface area AgCl/TiO_2-coupled photocatalytic cylinder. Bolts are used to spin the upper surface of the photocatalyst cylinder for the upper PLA plate to be combined tightly with the AgCl/TiO_2-coupled photocatalytic cylinder. Finally, near-ultraviolet light is irradiated to generate photoreduction to prepare a highly specific surface area Ag/AgCl/TiO_2-coupled photocatalytic module.

2.3 Three-dimensional printing of the TiO_2 photocatalyst cylinder

A self-made 3D printer created through FFF was used to print the TiO_2 photocatalyst cylinder. Commercial slicing software can be used to set printing parameters and generate G codes for printing devices by adopting 3D computer-aided design models. In the present study, the print head speed was 10 mm/s, the print bed temperature was 25°C, the print layer height was 0.14 mm, the nozzle temperature was 200°C, the (x, y) expansion factor was 19.87%, the z expansion factor was 25.32%, the filling was 30%, and the temperature of printing tablet was 80°C. Fused deposition printing was conducted on a 304 stainless steel printing substrate. With regard to the positioning system, the spatial resolution of the z-axis was approximately 100 m, and that of the x-axis and y-axis was approximately 11 m. Because of the brittleness of the 3D printing line, the entire fused deposition printing system had to be maintained at 50°C to increase its toughness. This green compact was solvent degreased in n-hexane at 60°C for 2 h to dissolve and remove the wax and open the pores. At this time, high-density polyethylene was used to maintain the shape of the green compact. Heat degreasing was then conducted for 1 h at 350 and 500°C to remove any remaining organic matter. The degreased green compact was then sintered in a high temperature furnace at 10^{-1} bar and 1200°C for 0.5 h to form dense TiO_2 photocatalyst cylinders.

2.4 Manufacturing of coupled Ag/AgCl/TiO_2

We used a heterogeneous precipitation reaction to prepare the Ag/AgCl/TiO_2-coupled photocatalytic structure (Figure 2). The preparation of the Ag/AgCl/ TiO_2 coupled photocatalyst is described in the following text. First, atmospheric-pressure plasma (5 kg/cm^2 of air at 220 V) was used to hydrophilize the surface of the sintered TiO_2 photocatalyst cylinder, which was then immersed in a 2.5 M aqueous NaCl solution. The NaCl solution was allowed to wet the hydrophilic surface of the TiO_2 photocatalyst completely, and the TiO_2 photocatalyst was then immersed in a 0.5 M aqueous $AgNO_3$ solution to cause a heterogeneous precipitation reaction. The precipitated AgCl film was evenly coated on the surface of the sintered TiO_2 photocatalyst cylinder. After drying for 2 h at 80°C, and then washed with deionized water several times to remove any residual chemicals from the surface of the cylinder. Next, to increase the strength of the coupling bond between the AgCl film and TiO_2, the AgCl/TiO_2 photocatalyst cylinder was placed in a high-temperature furnace at 430°C, heated at a heating rate of 5°C/min for 24 h, and then cooled to room temperature. Subsequently, this cylinder was irradiated with 365-nm ultraviolet light for 5 min to photoreduce AgCl to Ag/AgCl. Finally, we prepared a photocatalyst cylinder coupled with Ag/AgCl/TiO_2 as shown in Figure 1(b). The X-ray diffractometer (BRUKER, D8A) which was operated at

incident light with wavelength 1.54056 Å (CuKα) by copper target, scanning angle 2θ from 10° to 90°, a scanning rate of 0.1° s^{-1}, was used to compare and analyze the phases of crystalline phase of the sintered-TiO_2 and the Ag/AgCl/TiO_2-coupled photocatalyst [Joint Committee on Powder Diffraction Standards (JCPDS): 87e0597), AgCl (JCPDS: 85e1355), and anatase-phase TiO_2 (JCPDS: 71e1166).

2.5 Degradation of Orange II by Ag/AgCl/TiO_2 coupled photocatalytic module

The photocatalytic performance of the ceramic module produced through FFF was studied by adopting the Ag/AgCl/TiO_2 coupled photocatalytic module in the degradation of MB dye. MB dye was dissolved in deionized water to a concentration of 10 ppm. An ultraviolet light source (wavelength of 365 nm) and a visible light source (wavelengths of 435, 545, and 612 nm) with an output power of 9 W were used as the light sources for degradation. Fig. 3a and b depicts the UV and visible light spectrums, respectively. The ultraviolet and visible light sources were used simultaneously because the Ag/AgCl/TiO_2 coupled photocatalyst could absorb ultraviolet and visible light and decompose water simultaneously to produce a large quantity of highly active •OH and $•O_2^-$ for photocatalysis. Three blank tests were conducted to determine the photocatalytic abilities of the Ag/AgCl/TiO_2 coupled photocatalyst module and light sources. The setup and testing of the sintered module produced through FFF are described in the following text. A 500-mL glass beaker was used as a reactor and placed on a thermostat to maintain its temperature at 25°C. In each experiment, the concentration of the MB dye solution was 10 ppm, and the mixture was constantly stirred to increase the collision of dye molecules with the Ag/AgCl/TiO_2 coupled photocatalyst module. Dye degradation was investigated using three experiments. In the first experiment, only the ability of H_2O_2 to degrade MB dye was studied. In the other two experiments, the Ag/AgCl/TiO_2-coupled photocatalyst was hung in the dye solution, and a water lever was placed just above the photocatalysts. Both UV and visible light were placed near the glass beaker, as illustrated in Figure 4(a). In all the experiments, after irradiation, samples were collected regularly to analyze the degradation rate of the MB dye solution. The concentration of the degraded MB dye was measured in accordance with the NIEA W223.50B standard method, in which a spectrophotometer is used to measure the absorbance of a solution at different wavelengths to calculate its American Dye Manufacturers Association value.

2.6 Disinfection of *E. coli* by Ag/AgCl/TiO_2 coupled photocatalytic module

The ability of the sintered module produced through FFF to disinfect *E. coli* was similar to its ability to degrade MB dye. *E. coli* cultures with a concentration of 0.6 to 0.8 M were prepared in liquid nutrient broth (lysogen broth) at an optical density of 600 nm. Subsequently, a photocatalytic reaction was conducted for a predetermined duration on the sintered module produced through FFF under ultraviolet light (9 W; 365 nm) and visible light (9 W; 435, 545, and 612 nm) irradiation. Fig. 4b depicts the experimental setup for the photocatalytic disinfection of *E. coli*. The number of bacteria was determined through the establishment of the colony forming number (colony forming unit) by 1) diluting the samples (known

dilution ratio), 2) removing 100 µL of the diluted solution, and 3) smearing the samples on a nutrient agar Petri dish for a 24-h incubation period (37°C). The bacteria colony then grew, and the number of bacteria in the Petri dish was counted. Each set of the experiment was triple sampled within a predetermined period, cultivated, and counted for accuracy. Blank tests were also conducted for accuracy.

3 Results And Discussion

3.1 Characteristics of the 3D printing spool

The microstructures of the sintered TiO_2 and $AgCl/TiO_2$ photocatalysts are depicted in Fig. 5a and b, respectively. The average grain size of TiO_2 after sintering was approximately 8 µm, and AgCl particles with an average diameter of 20 nm were scattered on the surface of the filament, and the presence of Ag on the AgCl surface was identified through energy dispersive spectroscopy (EDS) and a mapping analysis [Figure 5 (c) and (d)]. Fig. 6 depicts the X-ray diffraction results obtained for the sintered TiO_2 and $Ag/AgCl/TiO_2$ coupled photocatalysts. According to the JCPDS database, the diffraction angles (with Miller indices in parentheses) of the sintered TiO_2 were 25° (101), 38° (004), 48° (200), 54° (105), and 55° (201). The diffraction angles of the Ag/AgCl crystals were 28° (111), 32° (200) and 46° (220). Moreover, the reduced form of the Ag clusters exhibited a diffraction angle of 38° (111).

3.2 Degradation of Orange II

In the 120-min blank test without light irradiation (only the $Ag/AgCl/TiO_2$ coupled photocatalyst module was used), the degradation rate was less than 2%, which indicates that the $Ag/AgCl/TiO_2$ photocatalyst can only be activated under light irradiation. Fig. 7 displays the concentration–time relationships for three types of photocatalysis: 10 ppm of MB + 10 mM hydrogen peroxide + the photocatalyst module (reaction A), 10 ppm of MB + the photocatalyst module (reaction B), and 10 ppm of MB + 10 mM hydrogen peroxide (reaction C). In this figure, C represents the concentration of MB dye at time t, and C_0 represents the initial concentration of 10 mg/L. In this study, the reaction rate followed first-order (or quasi–first order) kinetics [22]; thus, the equation $\ln(C/C_0) = k_{app} \times t$, where k_{app} is the apparent rate constant, which represents the degradation rate of MB dye, can be used to determine the catalytic performance. The k_{app} values of MB dye in reactions A, B, and C were 0.03754, 0.01149, and 0.004635 min^{-1}, respectively. Fig. 8b depicts the hyperbolic relationship for MB dye degradation ($C/C_0 = 1 - t/(a + bt)$ or $t/[1 - (C/C_0)] = a + bt$, where a and b are constants related to catalytic properties). The values of correlation coefficient R^2 (a, b) for reactions B and C were 0.9993 (6.777, 0.9423) and 0.9944 (40.28, 1.004), respectively. The R^2 values of the reactions were greater than 0.99, which indicates that the tests performed were more likely to accord with the hyperbolic kinetics relations than pseudo-first-order kinetics. When immersed into an aqueous MB dye solution containing 10 mM hydrogen peroxide, the $Ag/AgCl/TiO_2$ coupled photocatalyst almost completely degraded MB dye within 100 min (99% degradation). Fig. 8 illustrates the mechanism through which the $Ag/AgCl/TiO_2$ coupling photocatalyst degraded the MB dye. The degradation was related to the formation of strong oxidizing free radicals, such as O_2^-, on account of the interactions of

electrons (e^-) with surface O_2^- atoms. The electron holes (h^+) of AgCl can react with OH^- to generate OH^- radicals. $\bullet O_2^-$ and $\bullet OH^-$ are strong oxidants that can decompose MB dye (an organic compound) into CO_2 and water. In addition, some electron holes may react with AgCl and produce Ag^+ and ClO, where Ag^+ accepts electrons from the conduction band and forms Ag atoms and Ag clusters, which prevents further catalysis by AgCl. Cl^0 is also a strong oxidant and can decompose MB dye to generate CO_2, H_2O, and Cl^-. Moreover, H_2O_2 can increase the formation of OH^- free radicals and thus the degradation of MB dye. The surface plasmon resonance reaction of the Ag cluster on AgCl may absorb visible light intensively, thus leading to the increased production of Ag^+ and e^-, with some Ag^+ and Cl^- materials combining to reform AgCl. Additional, most of the electrons can flow from TiO_2 to AgCl to Ag clusters, mainly because the Fermi level of TiO_2 (4.89 eV) is higher than that of AgCl (4.6 eV) and Ag clusters (4.28 eV). Therefore, Ag clusters have too many electrons, while TiO_2 has too many holes, so the recombination of electrons and holes of Ag/TiO_2 can be prevented, which is beneficial to improve the performance of the photocatalyst. This phenomenon results in a highly stable and repeatable condition under which the reuse of this photocatalyst is feasible. Under UV and visible light conditions with five cycles of reuse, when the $Ag/AgCl/TiO_2$–coupled photocatalyst (cleaned with distilled water and air-dried before each use) was used, the degradability remained at 94%, as illustrated in Figure 9. This module therefore has high stability and durability.

3.3 Disinfection of *E. coli*

A photograph of the process of disinfecting *E. coli* by using the module produced through FFF is displayed in Fig. 10. Fig. 11a presents hyperbolic relationship between time and the number of colonies formed of different types of *E. coli* ($C/C_0 = 1 - t/(a + bt)$ or $t/[1 - (C/C_0)] = a + bt$). The values of a, b, and R^2 for the disinfection of *E.* coli were 2.255, 0.9868, and 0.9995, respectively. Almost all the *E. coli* was eliminated in 120 min when the $Ag/AgCl/TiO_2$ coupled photocatalyst was used. The disinfection efficiency is presented in terms of percentage in Fig. 12b. The mechanism of *E. coli* disinfection may be related to the generation of silver atoms or free radicals when ultraviolet or visible light photons hit the photocatalyst. When silver atoms come into contact with *E. coli*, some phosphoryl amino acids (such as phosphoryl tyrosine) are dephosphorylated, which results in a change in or the stoppage of the original function of the protein; thus, the growth rate of *E. coli* is reduced. The generated free radicals act as strong oxidants and can damage the cell wall, thereby causing essential substances (such as protein, glucose, and potassium ions) to leak from the cytoplasm into the external environment. Thus, these radicals may severely reduce cell membrane potential, adenosine triphosphate levels, and cell membrane permeability, which may lead to dysfunction or death. Silver nanoparticles may penetrate the cell membrane and bind to the thiol groups of certain enzymes (such as dehydrogenase) in the cell, thereby stopping the function of these enzymes and inactivating the basic metabolism of the cell. In a humid environment, Ag^+ and electrons may be released from Ag clusters and react with O_2 in water to form O_2–, H_2O, or •OH. These strong free radicals can effectively inhibit the metabolism of most cells. When Ag^+ interacts with bacteria, it may combine with the sulfhydryl group (-SH) in the protein, thereby breaking the

original disulfide bond (-S-S-) into a denatured state (-SAg). Ag^+ eventually stops all reactions related to cell respiration or electron transport, which results in cell death. After cell destruction, Ag^+ is released, which results in the death of additional cells. This process enables $Ag/AgCl/TiO_2$ to disinfect bacteria repeatedly and effectively. In the blank test (no light radiation), $Ag/AgCl/TiO_2$ had no effect on the growth of *E. coli*, which indicates that photons play a role in the activation reaction of $Ag/AgCl/TiO_2$ [23-24].

4 Conclusions

We fabricated a large–surface area $Ag/AgCl/TiO_2$ coupled photocatalytic module by 3D-printing a ceramic module produced through FFF. The photocatalytic ability of the $Ag/AgCl/TiO_2$ coupled photocatalytic module to degrade MB dye and disinfect *E. coli* under ultraviolet and visible light irradiation was also studied. This module is suitable for degrading MB dye and disinfecting *E. coli* within a few minutes to a few hours, depending on the specific surface area of the module. After five cycles of repeated use, the module's ability to degrade dyes and bacteria remains high (95%). A module based on $Ag/AgCl/TiO_2$ produced through FFF has broad application prospects as a photocatalyst for degrading pollutants because of its effectiveness, reliability, and structural durability.

Declarations

Funding

This study was supported by the National Science Council, Taiwan (MOST109-2221-E-032-021).

Author information

Affiliations

1. Department of Mechanical and Electro-Mechanical Engineering, Tamkang University, Tamsui, New Taipei, Taiwan, R.O.C.

Zheng-Rong Yang□Chun-Yu Kuo□Chung-Hao Shin□Ching-Bin Lin

2. Department of Water Resources and Environmental Engineering, Tamkang University, Tamsui, New Taipei, Taiwan, R.O.C.

Po-Ching Lee

Corresponding author

Correspondence to Ching-Bin Lin

Ethics declarations

Author contribution

All the authors have contributed equally to the paper.

Ethics approval

Complied with ethical standards.

Consent to participate and consent to publish

All authors agree to contribute and publish the article.

Competing interests

The authors declare no competing interests.

References

1.Huang S T, Jiang Y R, Chou S Y, Dai Y M, Chen C C (2014) Synthesis, characterization, photocatalytic activity of visible-light-responsive photocatalysts BiO_xCl_y/BiO_mBr_n by controlled hydrothermal method. J. Mol. Catal. A: Chem.391(1):105-120. https://doi.org/10.1016/j.molcata.2014.04.020

2.Low J, Yu J, Jaroniec M, Wageh S, Al-Ghandi A A. (2017) Heterojunction Photocatalysts. Adv. Mater. 29(20):1601694. https://doi.org/10.1002/adma. 201601694

3.Fujisima A, Hinda K. (1972) Electrochemical Photolysis of Water at a Semiconductor Electrode. Nature 238:37-38 https://doi.org/10.1038/238037a0

4.Libanori R, Giraldi T R, Longo E, Leite E R (2009) Effect of TiO_2 surface modification in Rhodamine B photodegradation. J. Sol. Gel. Sci. Technol. 49(1):95-100 https://doi.org/10.1007/s10971-008-1821-1

5.Choi M, Shin K H, Jang J (2010) Plasmonic photocatalytic system using silver chloride/silver nanostructures under visible light. J. Colloid Interface Sci. 341(1):83-87(5) https://doi.org/10.1016/j.jcis.2009.09.037

6. Kakuta N, Goto N, Ohkita H, Mizushima T (1999) Silver Bromide as a Photocatalyst for Hydrogen Generation from CH_3OH/H_2O Solution. J. Phys. Chem. B 103(29):5917-5919. https://doi.org/10.1021/jp990287q

7.Guo J F, Ma B W, Yin A Y, Fan K N, Dai W L (2012) Highly stable and efficient $Ag/AgCl@TiO_2$ photocatalyst: Preparation, characterization, and application in the treatment of aqueous hazardous pollutants. J. Hazard. Mater.211-212:77-82. https://doi.org/10.1016/j.jhazmat.2011.11.082

8.Sohrabnezhad S, Pourahmad A (2012) As-synthesis of nanostructure AgCl/Ag/MCM-41 composite. Spectrochim. Acta A Mol. Biomol. Spectrosc. 86:271-275. https://doi.org/10.1016/j.saa.2011.10.035

9.Yang Q, Hu M, Guo J, Ge Z, Feng J (2018) Synthesis and enhanced photocatalytic performance of Ag/AgCl/TiO_2 nanocomposites prepared by ion exchange method. J. Materiomics 4(4):402-411. https://doi.org/10.1016/j.jmat.2018.06.002

10.Hu C, Peng T W, Hu X X, Nie Y L, Zhou X F, Qu J H, He H (2010) Plasmon-Induced Photodegradation of Toxic Pollutants with Ag–AgI/Al_2O_3 under Visible-Light Irradiation. J. Am. Chem. Soc., 132(2):857-862. https://doi.org/10.1021/ja907792d

11.Xu Y G, Xu H, Li H M, Xia J X, Liu C T, Liu L (2011) Enhanced photocatalytic activity of new photocatalyst Ag/AgCl/ZnO. J. Alloys Compd.509(7):3286-3292. https://doi.org/10.1016/j.jallcom.2010.11.193

12.Luo G Q, Jiang X J, Li M J, Shen Q, Zhang L M, Yu H G (2013) Facile Fabrication and Enhanced Photocatalytic Performance of Ag/AgCl/rGO Heterostructure Photocatalyst. ACS Appl. Mater. Interfaces 5(6):2161-2168. https://doi.org/10.1021/ am303225n.

13. Henrika Granbohm, Vivek K. Singh, Yanling Ge and Simo-Pekka Hannula(2017) Effect of graphene oxide loading in GO/SiO2/Ag/AgCl photocatalystInt. J. Nanotechnol., 14: pp 87-99. https://doi.org/10.1504/ijnt.2017.082448

14. Priyanka Panchal, Poonam Meena, Satya Pal Nehra (2021) rapid green synthesis of Ag/AgCl-NC photocatalyst for environmental applications. Environmental Science and Pollution Research 28:3972–3982doi:10.1007/s11356-020-11834-5.

15. Vandana P. Viswanathan, K. S. Divya, Deepak P. Dubal, Nayarassery N. Adarsh and Suresh Mathew (2021) Ag/AgCl@MIL-88A(Fe) heterojunction ternary composites: towards the photocatalytic degradation of organic pollutants. Dalton Trans. **50:**2891-2902 https://doi.org/10.1039/D0DT03147J

16.Zhang J, Liu X, Suo X, Li P, Liu B, Shi H (2017) Facile synthesis of Ag/AgCl/TiO_2 plasmonic photocatalyst with efficiently antibacterial activity. Mater. Lett. 198:164-167. https://doi.org/10.1016/j.matlet.2017.04.029

17.Liu W, Chen D, Yoo S, Cho S (2013). Hierarchical visible-light-response Ag/AgCl@TiO_2 plasmonic photocatalysts for organic dye degradation. Nanotechnology 24(40):405706. https://doi.org/10.1088/0957-4484/24/40/405706

18.Shah Z, Wang J S, Ge X, Wang C, Mao W, Zhang. S (2015) Highly enhanced plasmonic photocatalytic activity of Ag/AgCl/TiO_2 by CuO co-catalyst. J. Mater. Chem. A 3(7):3568-3575. https://doi.org/10.1039/c4ta05777e

19.Ge Z, Ji Y, Qiu Y, Chong X, Feng J, He J (2018) Enhanced thermoelectric properties of bismuth telluride bulk achieved by telluride-spilling during the spark plasma sintering process. Scripta. Mater.143:90-93. https://doi.org/10.1016/j.scriptamat. 2017.09.020

20.Yang L, Ma X, Zhang W, Gen W (2016) Ag@AgCl-TiO_2/organic rectorite/quaternized chitosan microspheres: An efficient and environmental photocatalyst. J. Appl. Polym. Sci. 134:44601. https://doi.org/10.1002/app.44601

21. Xinmei Guan, Shaojian Lin, Jianwu Lan, Jiaojiao Shang, Wenxu Li, Yifei Zhan, Hongyan Xiao and Qingshuang Song (2019) Fabrication of Ag/AgCl/ZIF-8/TiO2 decorated cotton fabric as a highly efficient photocatalyst for degradation of organic dyes under visible light. Cellulose 26(12):7437-7450.http://doi.org/10.1007/s10570-019-02621-8

22. Saien J, Khezrianjoo S (2008) Degradation of the fungicide carbendazim in aqueous solutions with UV/TiO_2 process: Optimization, kinetics and toxicity studies, J. Hazard. Mater.157(2-3):269-276. https://doi.org/10.1016/j.jhazmat.2007.12.094

23.Wang D, Li Y, Puma G L, Wang C, Wang P, Zhanga W, Wang Q (2015) Mechanism and experimental study on the photocatalytic performance of Ag/AgCl @ chiral TiO_2 nanofibers photocatalyst: The impact of wastewater components. J. Hazard. Mater. 285:277-84. https://doi.org/10.1016/j.jhazmat.2014.10.060

24.Nie L, Hu B, Jiang J (2012) Preparation of Ag/AgCl/TiO_2-XCX Plasmonic Photo-Catalyst with Enhanced Visible-Light Photocatalytic Activity. Adv. Mater. Res.356-360:506-509. https://doi.org/10.4028/www.scientific.net/AMR.356-360.506

Figures

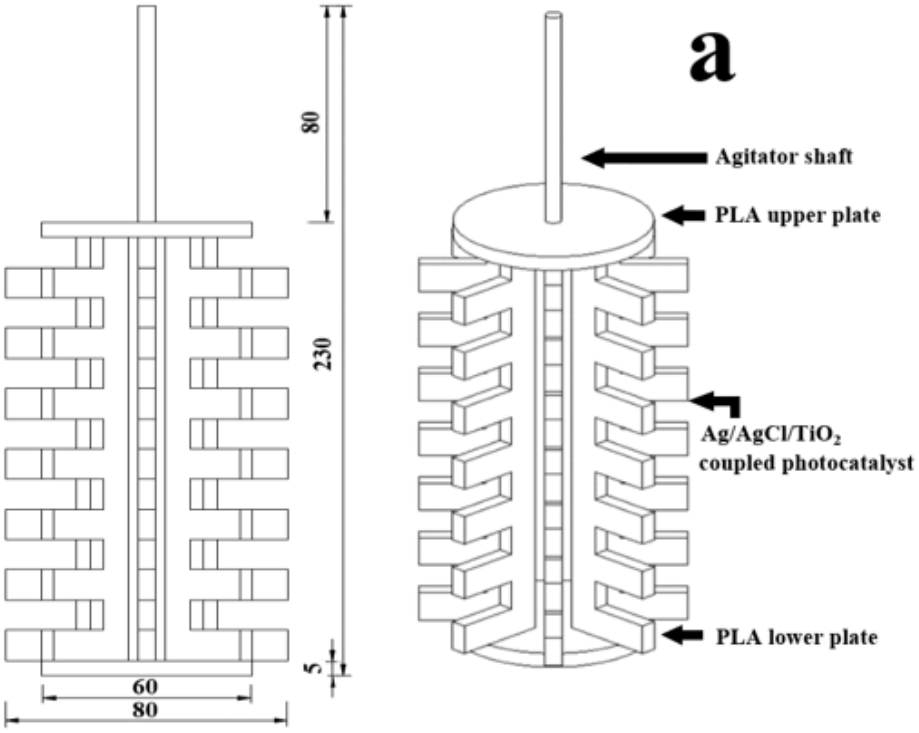

Figure 1

(a) Design of highly specific surface area Ag/AgCl/TiO_2-coupled photocatalyst; (b) Green compact structure of the sintered TiO_2 after fused deposition printing and (c) the Ag/AgCl/TiO_2 photocatalytic module (the module produced through FFF)

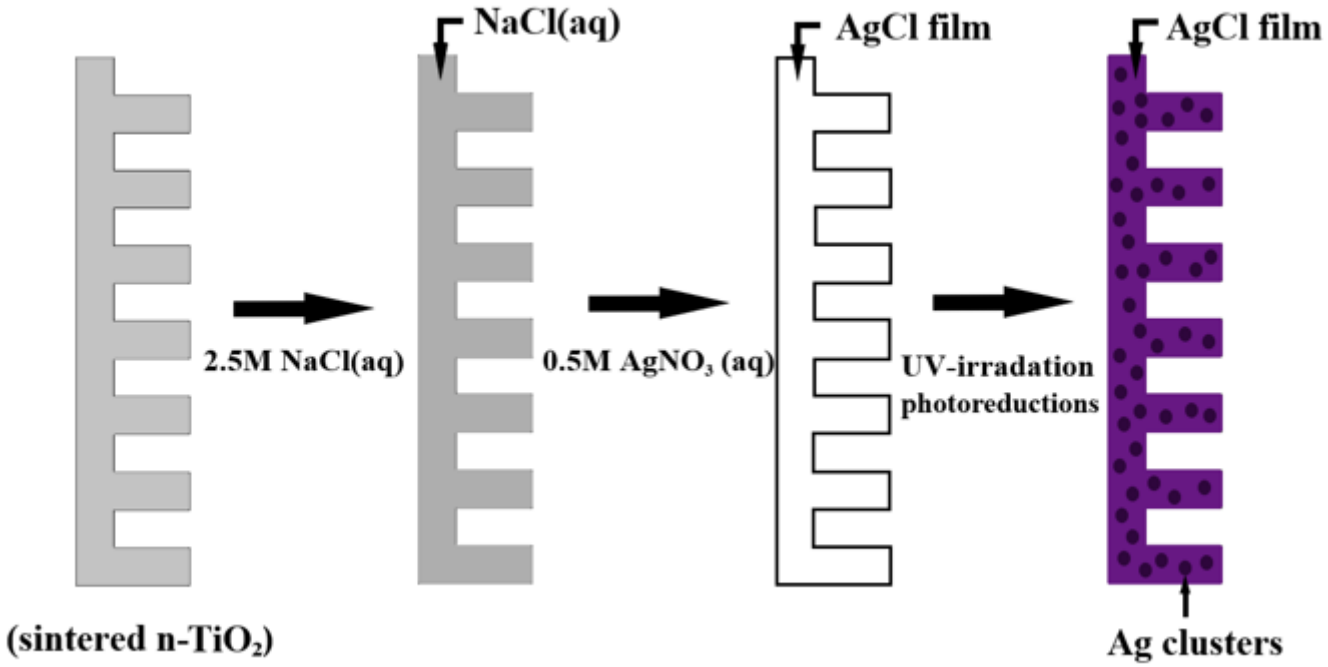

Figure 2

Precipitation method for preparing the Ag/AgCl/TiO_2 coupled photocatalyst

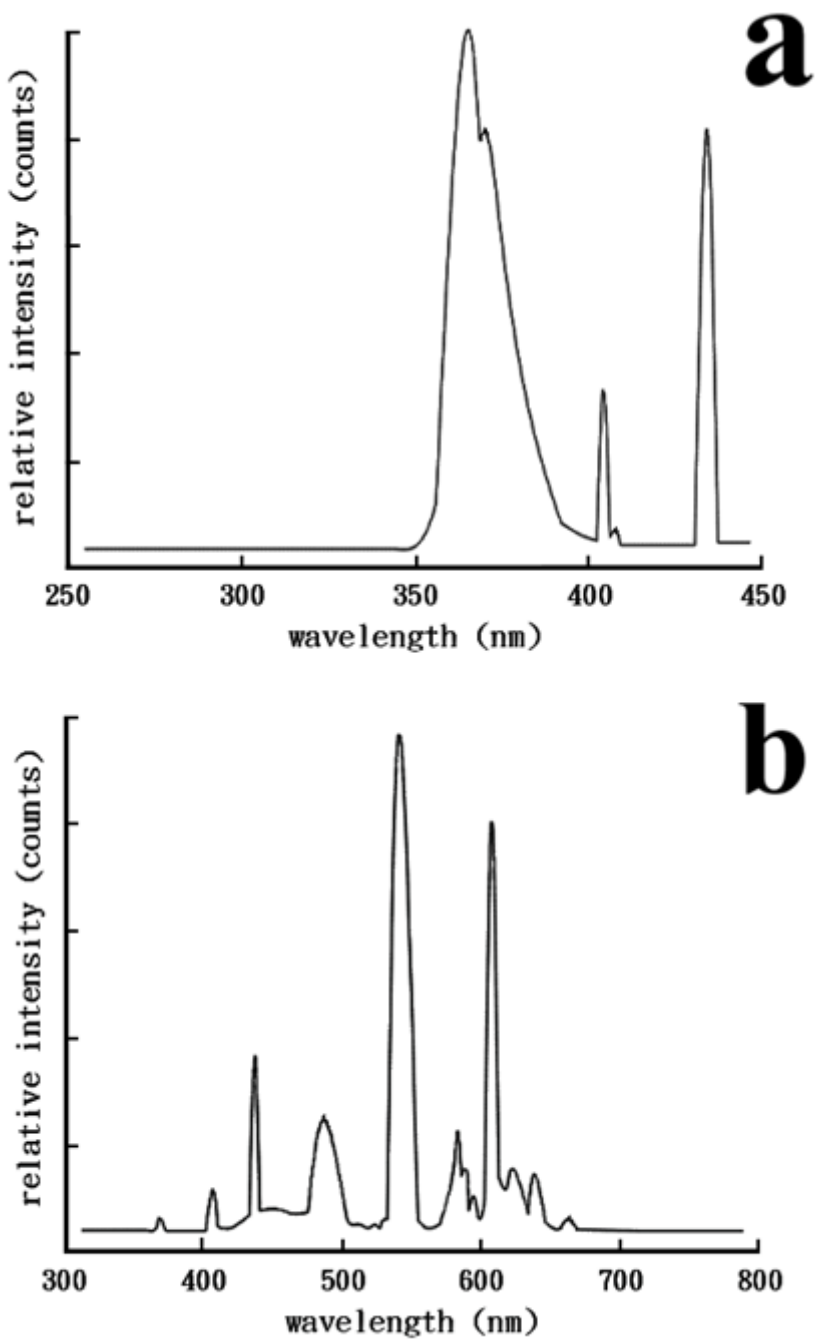

Figure 3

Light source spectrum of (a) UV light and (b) visible light

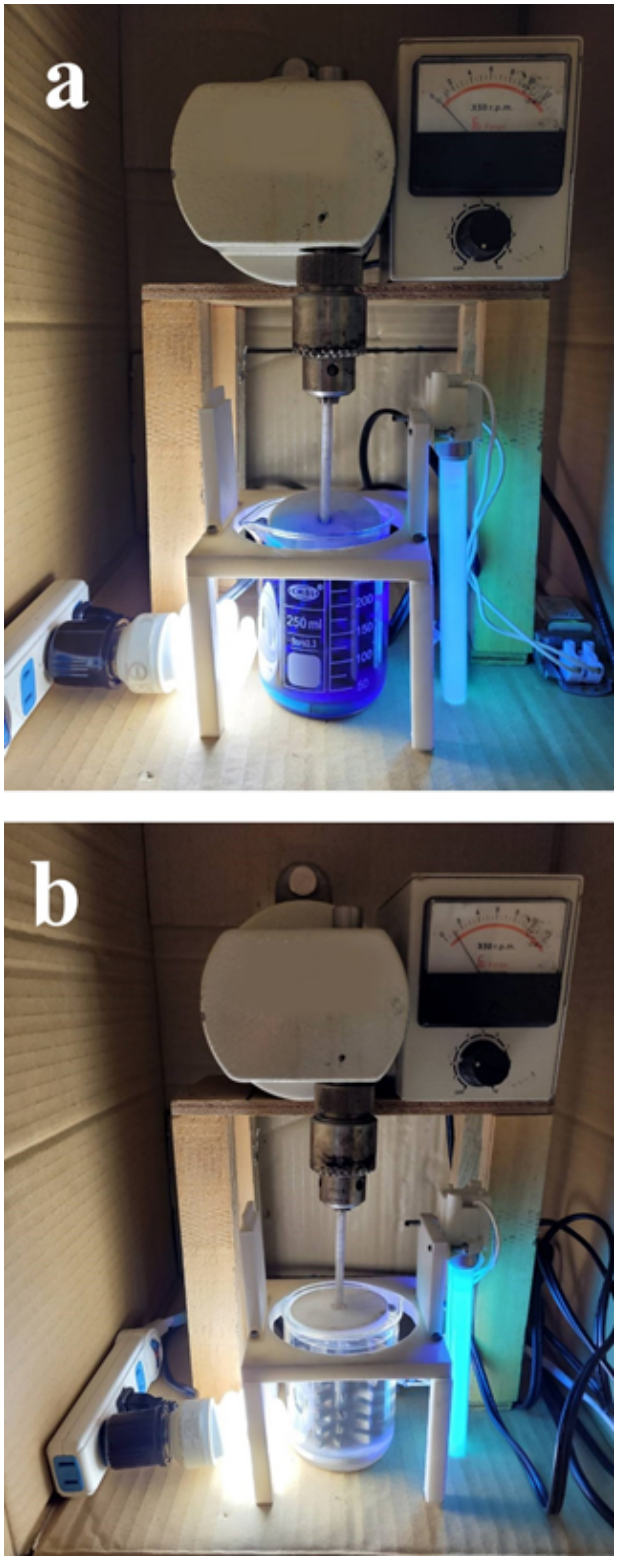

Figure 4

Setup for the (a) degradation of azo dye (Orange II) and (b) disinfection of *E. coli*

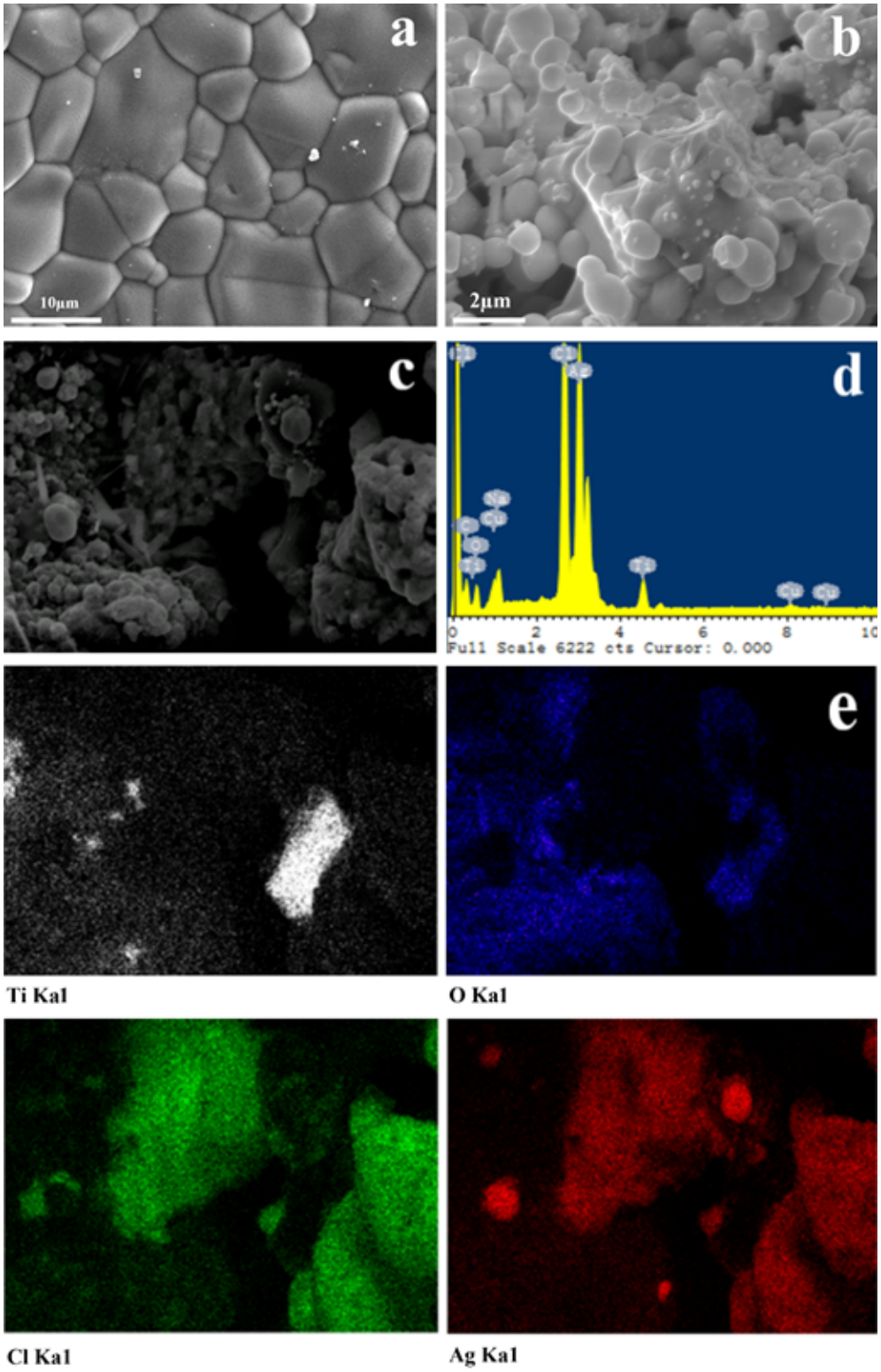

Figure 5

Microstructure of (a) sintered-TiO_2 and (b) Ag/AgCl/TiO_2-coupled photocatalyst Ti, O, Cl, and Ag identified using (c) energy dispersive spectroscopy and (d) mapping analysis

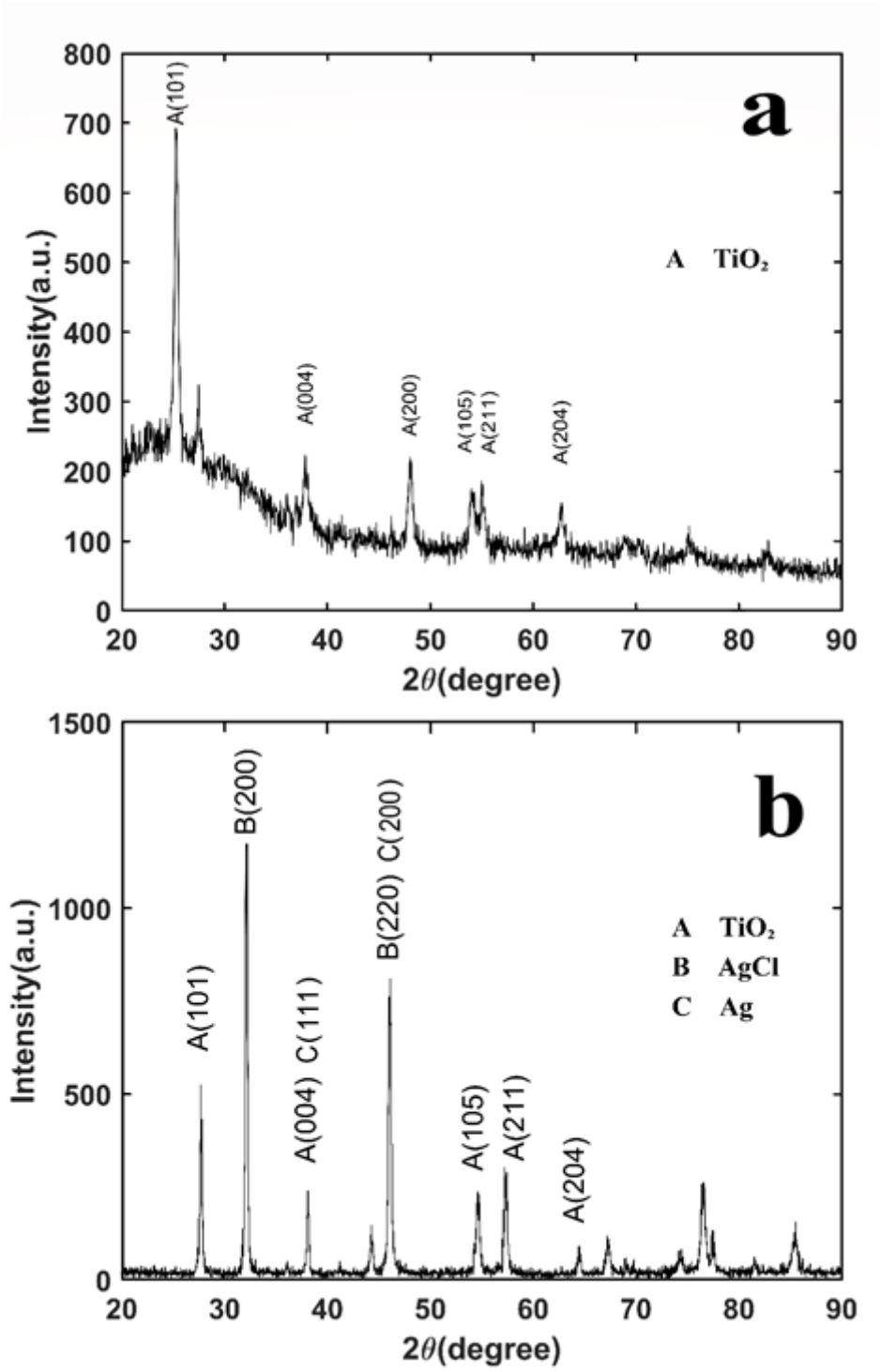

Figure 6

X-ray diffraction patterns of (a) TiO_2 and (b) the Ag/AgCl/TiO_2 photocatalyst

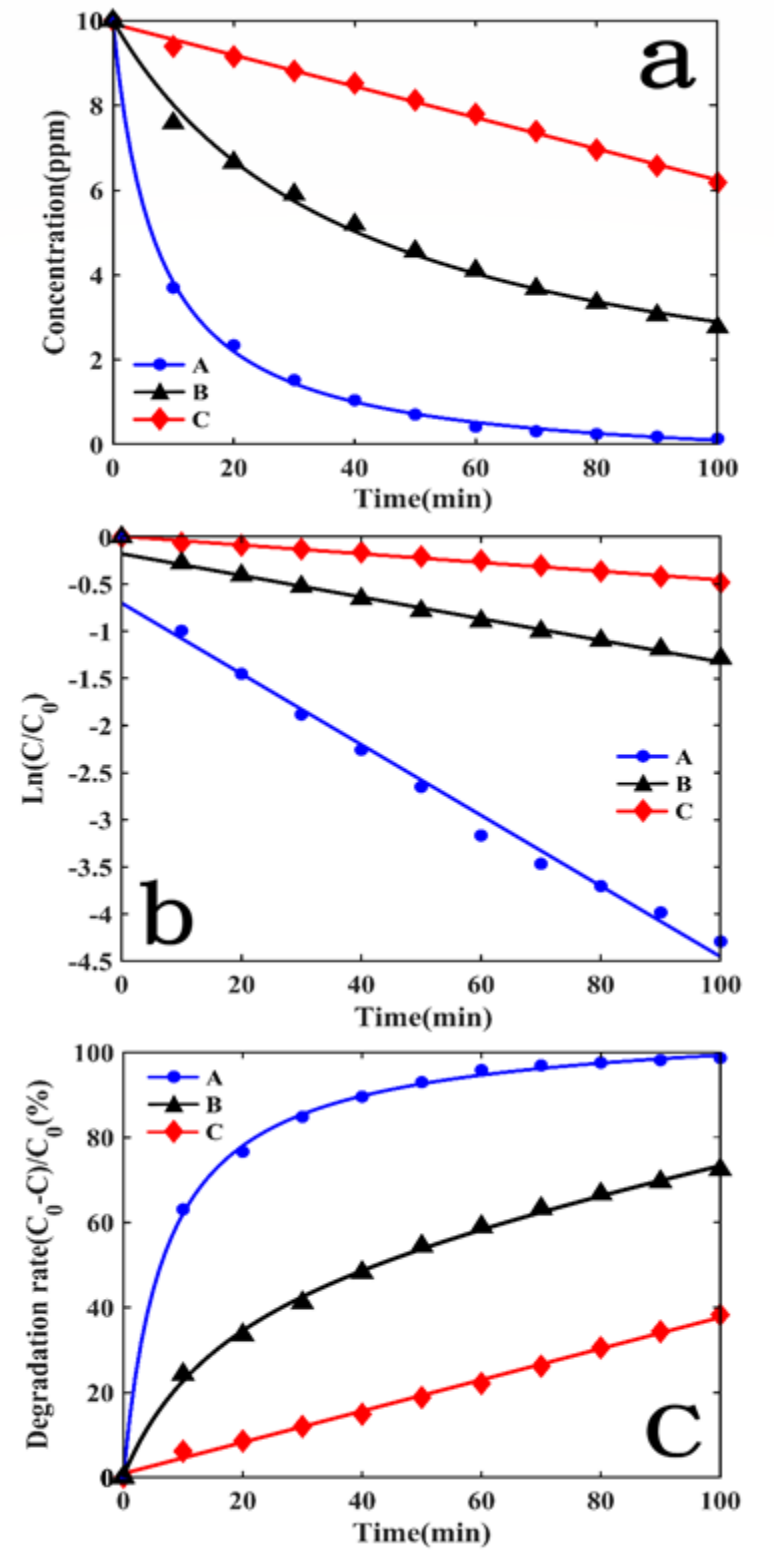

Figure 7

Degradability of MB dye performed on different scales. (a) Concentration variation over time; (b) concentration logarithm in relation to initial concentration over time; (c) degradation over time (residual concentration to initial concentration).

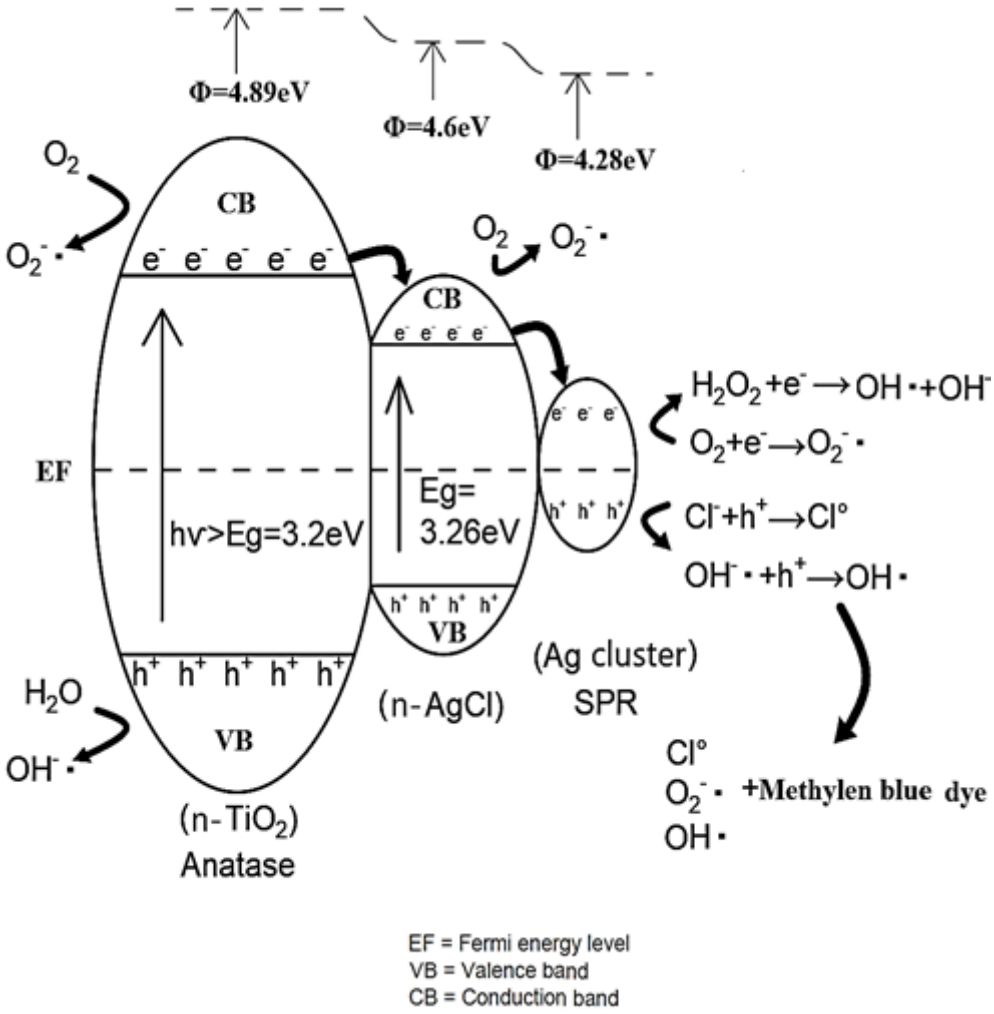

Figure 8

Mechanism of the photocatalytic reaction of Ag/AgCl/TiO_2

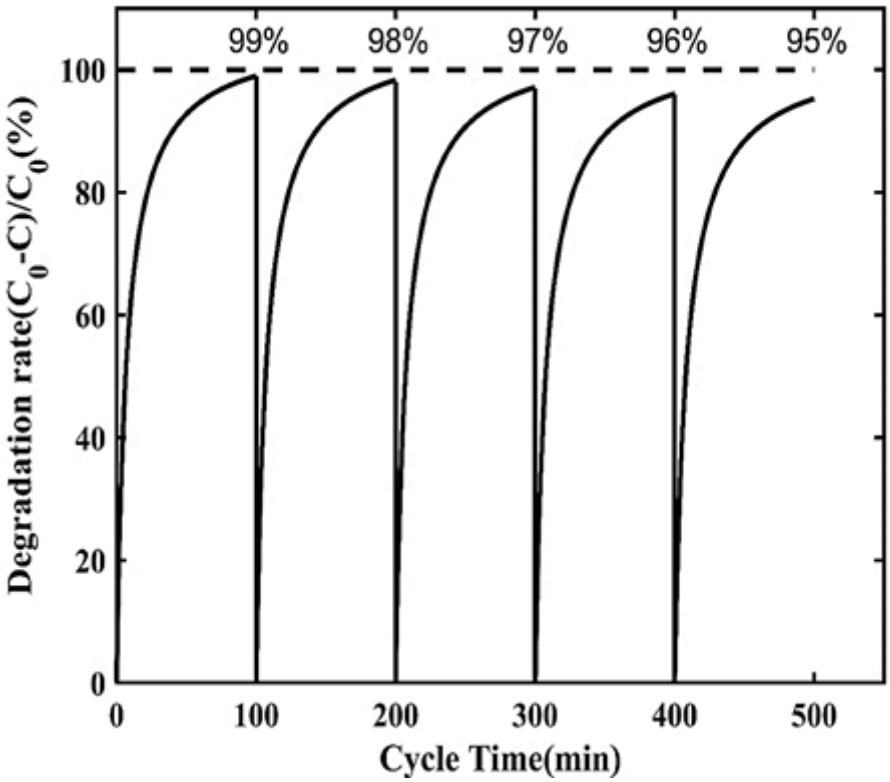

Figure 9

Degradation of MB upon five consecutive uses of the module produced through FFF

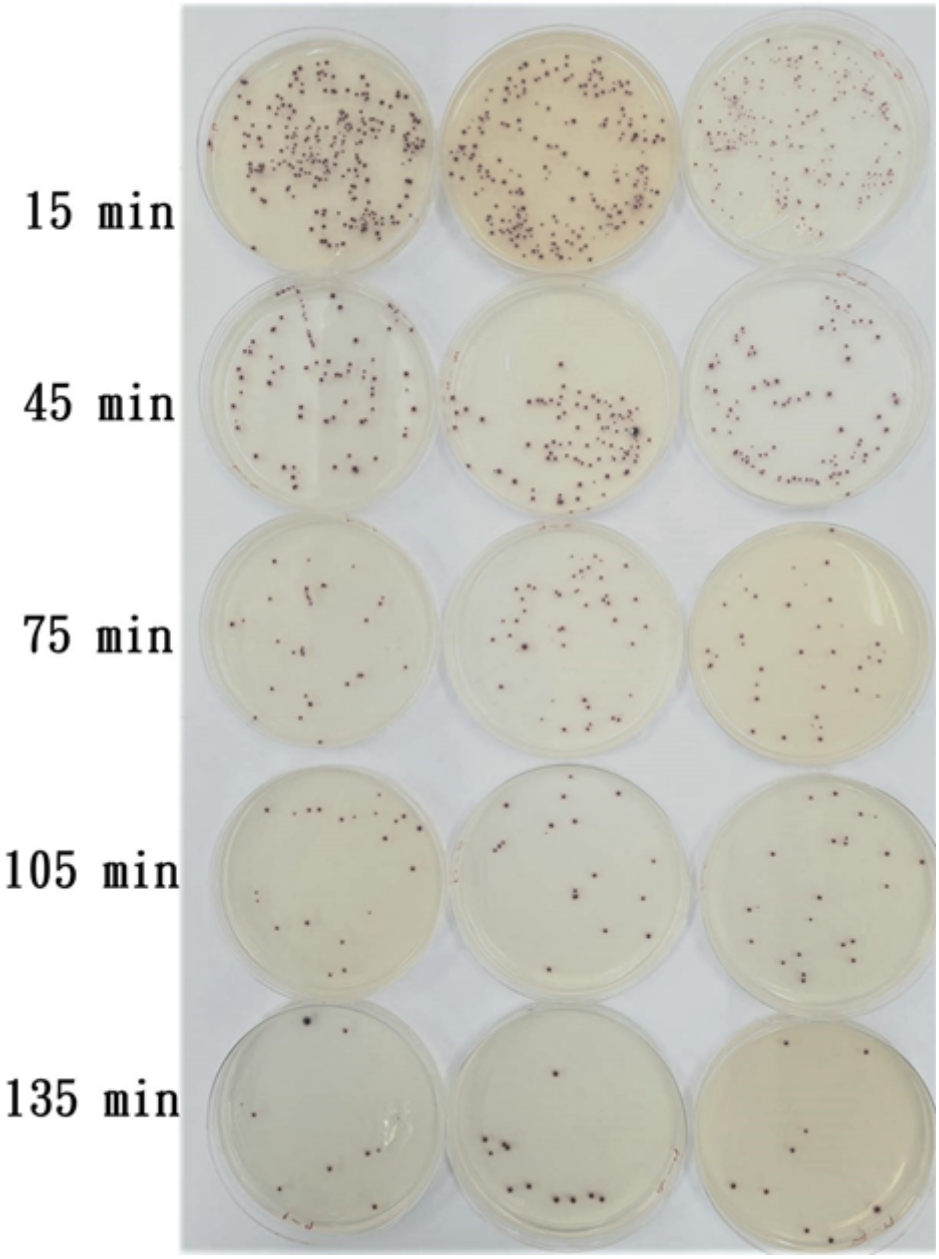

Figure 10

E. coli colony samples on a Petri dish after 15, 45, 75, 105, and 135 min of catalytic disinfection treatment

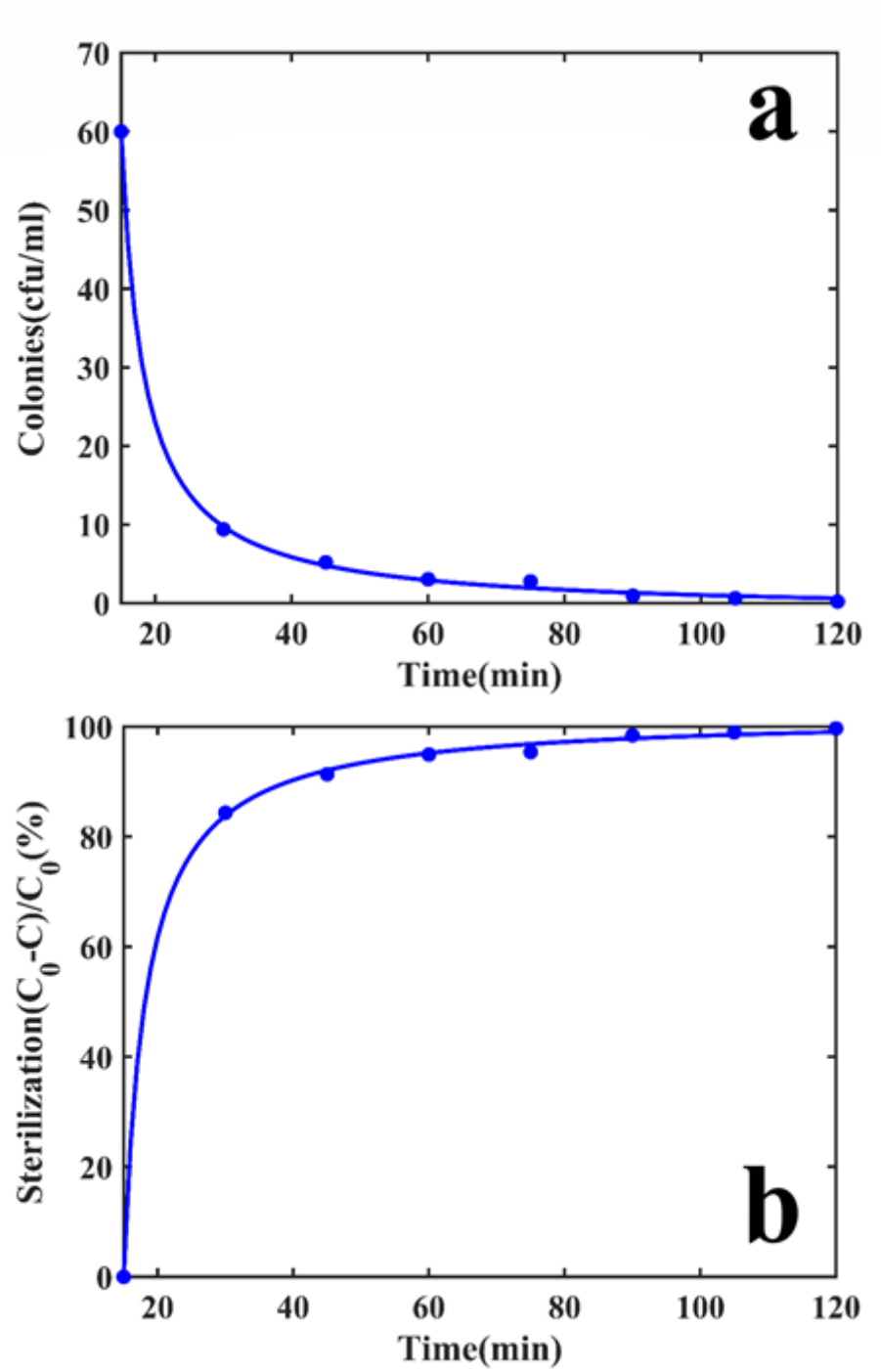

Figure 11

Disinfection of *E. coli*: (a) variation in the *E. coli* concentration over time and (b) time-dependent disinfection efficiency in terms of percentage (residual concentration to initial concentration)